Study of molecular structures, electronic properties, spectroscopic analysis and thermodynamic properties of Azulene using First-principles calculations

Tilak Khadka[*], Nirmal Bishwokarma[*], Prakash Man Shrestha[*], Rishi Ram Ghimire[*] and Krishna Bahadur Rai[*]

[*]Department of Physics, Patan Multiple Campus, Lalitpur, Tribhuvan University, Nepal.

Abstract: Density Functional Theory investigation of Azulene was carried out on the azulene molecule at the B3LYP/6-311G++(d,p) level using Gaussian 09. The optimized geometry confirmed structural stability with consistent bond parameters having the longest bond length of 1.49 Å for C7-C5 shortest bond length of 1.08 Å for C13-H14 and the largest bond angle of 129.89° for C4-C1-C2 indicating slight angular distortion in the carbon framework. The optimized total energy of Azulene is −385.935 Hartree (-10501.291 eV) to be in the optimized geometric structure geometry. The calculated HOMO-LUMO gap with value 3.287 eV agreed well with the density of states having 3.257 eV suggesting that azulene is relatively stable and less prone to electron transfer under normal conditions. Mulliken charge analysis shows that all the hydrogen atoms have positive charges and all of the carbon atom except C5 and C7 corresponds to the negative charge. H8 and H11 exhibit the highest positive charge, while the C1 and C2 exhibit the highest negative charge. The global reactivity descriptors like ionization potential, electron affinity, chemical potential, electronegativity, hardness, softness, and electrophilic index are found to be 5.557 eV, 2.269 eV, -3.931 eV, 3.931 eV, 1.644 eV, 0.608 eV^{-1} and 4.656 eV respectively. Molecular electrostatic potential, electrostatic surface potential and electron density analyses revealed distinct electron-rich and electron-deficient regions clarifying the molecule's reactive sites. Vibrational assignments were consistent with characteristic C-H and C=C modes and thermodynamic parameters demonstrated temperature-dependent increases in heat capacities, internal energy, enthalpy, and entropy, accompanied by a decrease in Gibbs free energy with respect to increase in temperature.

Keywords: Azulene; Density function theory; Electronic structures; Vibrational modes; Thermodynamic parameters.

Introduction

Azulene ($C_{10}H_8$) is a specific aromatic organic hydrocarbon obtained from merged rings designed of pentagon and heptagon. It's molecular formula is $C_{10}H_8$ and IUPAC name is bicyclo[5.3.0]deca-1,3,5,7,9-pentaene [1]. Its derivatives are extensively incorporated into pharmaceutical and cosmetic products because of their strong anti - inflammatory and soothing properties, particularly in the treatment of burns, wounds, skin irritation, and inflammatory conditions of the oral cavity and gums [2]. They are also being explored as potential agents for the treatment of cancer and various dermatological disorders, with studies focusing on their mechanisms of action and clinical outcomes [3]. It was found for application in molecular electronics, organic semiconductors as well as its structure sets it apart from regular fused benzenoids and enables the creation of complex optoelectronic materials [4]. It is a useful model system in spectroscopic analysis, photochemical, and computational chemistry investigations due to its unique aromatic and excited-state behavior, especially for

Author for correspondence: Krishna Bahadur Rai, Department of Physics, Patan Multiple Campus, Lalitpur, Tribhuvan University, Nepal.
Email: krishna.rai@pmc.tu.edu.np; https://orcid.org/0000-0001-8882-0385
Received: 22 Feb, 2026; Received in revised form: 21 Apr, 2026; Accepted: 28 Apr, 2026.
Doi: https://doi.org/10.3126/sw.v19i19.95588

tanding charge transfer, electronic structure, thermodynamic and UV–visible, infrared radiation [5]. Figure 1 shows chemical structure of Azulene and due to its unique chemical structure, a negatively charged 5-membered ring connected with a positively charged 7-membered ring, Azulene, a special isomer of naphthalene, has drawn the attention of scientists from a variety of disciplines [6].

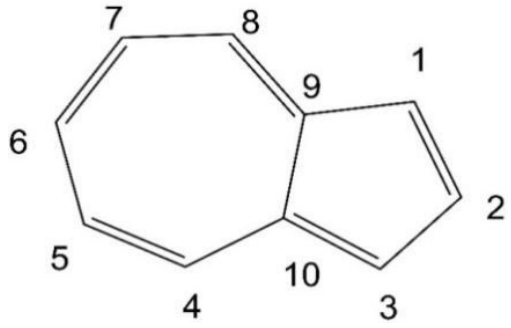

Figure 1: Chemical structure of Azulene.

Adding Azulene to polymers has produced a number of interesting characteristics with a dipole moment of 1.08 D due to resonance delocalization, as well as its different reactivity at odd and even positions and response to stimulus behavior [7] that have received more attention in recent years. The non-zero dipole moment (1.08 D) of azulene arises from its unique electronic structure. Unlike symmetric aromatic systems, azulene exhibits an uneven distribution of electron density, where electron transfer occurs from the seven-membered ring to the five-membered ring. This redistribution allows both rings to attain effective 6π aromatic stabilization. As a result, the five-membered ring becomes electron-rich while the seven-membered ring becomes electron-deficient, leading to a permanent dipole moment. Hajialiakbari et al. (2024) examined the aromatic structural characteristics of azulene and its monophosphate derivatives, assessing their reactivity by examining local electrophilicity and nucleophilicity indices [8]. Monophosphate derivatives are molecules that have a single phosphate group attached to them. Theoretical investigation using the 6-311++G(d,p) basis set conducted to the gas-phase basicity and acidity of an azulene-based uracil analogue determine the proton affinities of two oxygen and two nitrogen atoms as well as the deprotonation energies of two NH and two OH bonds [9]. The density functional theory in combination with the non-equilibrium Green's function technique determined electron transport in azulene, a non-alternative hydrocarbon [10]. However, Azulene's molecular structure, spectroscopic analysis, and thermodynamic properties have not yet been thoroughly investigated using Density Functional Theory (DFT) with the B3LYP method at 6-311G ++(d, p) basis set. To fulfil this gap, we study optimization structure, highest occupied molecular orbital (HOMO)-lowest unoccupied molecular orbital (LUMO) and its energy gap, density of states (DOS), Mulliken atomic charge, global reactivity index (GRI), electrostatic potential (ESP), molecular electrostatic potential (MEP), electron density (ED), vibrational analysis and thermodynamic parameters analysis of Azulene molecule.

Computational details

The Gaussian09W program and GaussView 6.0 were used for the quantum computation of the azulene molecule. Using the density functional theory (DFT) B3LYP method at the 6-311G++(d, p) basis set, the most optimal structure of the title molecule was visualized following the computation of bond length, bond angle, dihedral angle, HOMO-LUMO energy gap, Mulliken atomic charges, global reactivity index, MEP, ESP, ED, and spectroscopic characteristics (FT-IR). The GaussSum3.0 software was used to obtain the density of states (DOS) spectrum using the .log file. Moltran software for the .log file from the Gaussian software was also used for finding the relationship between thermodynamic parameters including heat capacity at constant volume (C_V), heat capacity at constant pressure (C_P), total internal energy (U), enthalpy (H), entropy (S), and Gibb's free energy (G) with respect to the temperature change.

According to Koopman's theorem, ionization potential (I) and electron affinity (A) are directly related to HOMO and LUMO energies, respectively [11]. The energy required to remove an electron from a gaseous atom is known as ionization energy (I). In an analogous way, the energy released when an additional electron is introduced to an

atom is measured by electron affinity (A). The relationship between ionization potential (I) and electron affinity (A) is shown below [12,13].

$$\text{Ionization Potential (I)} = -E_{HOMO} \ldots (1)$$

$$\text{Electron Affinity (A)} = -E_{LUMO} \ldots (2)$$

The global reactivity parameter index such as chemical Potential (μ), electronegativity (χ), global hardness (η), Softness (ζ) and electrophilicity index (ω) are calculated using the relation given below [14,15].

$$\text{Chemical potential } (\mu) = -(I+A)/2 \quad \ldots\ldots\ldots \quad (3)$$

$$\text{Electronegativity } (\chi) = (I+A)/2 \quad \ldots\ldots \quad (4)$$

$$\text{Global Hardness } (\eta) = (I-A)/2 \quad \ldots\ldots\ldots \quad (5)$$

$$\text{Softness } (S) = 1/\eta \quad \ldots\ldots\ldots \quad (6)$$

$$\text{Electrophilic Index } (\omega) = \mu^2/2\eta \quad \ldots\ldots \quad (7)$$

Results and Discussion

Optimized molecular structure

The $C_{10}H_8$ molecule's minimal energy configuration or ground state optimized geometry, together with atomic numbering, are shown in Figure 2(a) where the ground state energy of the molecule is the lowest and it is stable. This Figure 2(b) illustrates the relationship between energy and the number of optimization steps and it shows that the optimization energy state happens in seven distinct steps. The optimization energy of a molecule refers to the energy needed for it to reach its most stable and neutral state [16]. Azulene molecule starts to optimize from the energy -385.929 Hartree (-10501.128 eV) and this energy sharply drops to -385.934 Hartree (-10501.264 eV) in the first two steps. Once more, the energy gradually drops and it approaches Azulene's optimum energy equal to -385.935 Hatree (-10501.291 eV).

Calculation of bond length, bond angle and dihedral angle

The title molecule displays bond lengths, bond angles, and dihedral angles based on Gaussian calculations, as shown in Table 1. Dihedral angles can have both positive and negative values, however bond lengths and bond angles are always positive [17], positive and negative values in dihedral angles indicate the molecular conformation. Molecular conformation is the way atoms are arranged in space in a molecule. This can change by rotating around single bonds without breaking any of them. The distance between two connected atoms is represented by a bond length, three connected atoms by a bond angle, and four connected atoms by a dihedral angle [16,17]. The calculated bond length lies between the range 1.08 Å to 1.49 Å. The C-C bond lengths appeared between 1.38 Å to 1.49 Å, which are good agreement with the experimental values in the range 1.37 to 1.43 Å, while all C-H bond lengths are 1.08 Å, they are also in good agreement to experimental values ~1.09 Å. The bond length between C7-C5 is high value i.e. 1.49 Å and the length between C13-H14 is low i.e. 1.08 Å in B3LYP method. The average bond angle between C-C-C is 115˚ and C-C-H is 130˚. Similarly, dihedral angle is either 0 or around to ±180˚. From the experimental XRD data, the five member rings C-C bonds have bond length of 1.39 Å -1.40 Å range and C-C-C bond angle have values 106º-109º and this agrees well with the calculated values obtained using the DFT/B3LYP method at the 6-311G++(d, p) basis set. Similarly, the calculated data of bond length and bond angle for seven ring carbon are also matched with the experimental data of C-C bond length and C-C-C bond angle having values 1.51Å -1.54 Å and 126.7º-129.9º respectively [18].

Electronic properties

HOMO-LUMO analysis

It is required to evaluate highest occupied molecular orbital (HOMO) and lowest unoccupied molecular orbital (LUMO) calculation to understand the molecular electronic properties of the title molecule. The highest-energy molecular orbital that contains electrons and can donate them is called the HOMO. The lowest-energy molecular orbital that can accept electrons is known as the LUMO. They are also called frontier molecular orbitals [19]. A higher HOMO energy indicates a greater tendency to donate electrons, and vice versa. Similarly, a lower LUMO energy value signifies a stronger ability to accept electrons. The energy difference between the HOMO and LUMO is referred to as the energy gap. The energy gap between the HOMO and LUMO is an important parameter

for evaluating electron conductivity (mobility) [20]. A smaller HOMO-LUMO gap corresponds to enhanced electronic transition, whereas a larger gap indicates reduced transition probability [21, 22]. A positive energy gap indicates molecular stability, whereas a negative gap suggests instability [23]. Figure 3 illustrates the HOMO and LUMO energy values of the azulene molecule along with their energy gap. The calculated HOMO and LUMO energies are -5.557 eV and -2.269 eV, respectively, resulting in an energy gap of 3.287 eV. Thus, the HOMO-LUMO gap of the azulene molecule is reflecting considerable electronic stability. A larger gap generally implies lower chemical reactivity and higher kinetic stability, suggesting that $C_{10}H_8$ is relatively stable and less prone to electron transfer under normal conditions.

Azulene, an isomer of naphthalene, exhibits a significantly

Table 1: Optimized value of geometrical parameters of Azulene molecule.

Bond Length	Value (Å)	Bond angle	Value (◦)	Dihedral angle	Value (◦)
C1-C2	1.39	C4-C1-H8	115.07	C4-C1-C2-C3	0.00
C2-C3	1.39	C6-C4-H11	115.68	C2-C3-C5-C7	0.00
C3-C5	1.39	C1-C4-H11	115.63	C7-C6-C4-C1	0.00
C5-C13	1.40	C4-C6-H12	115.69	C7-C17-C15-C13	0.02
C13-C15	1.40	C7-C6-H12	115.29	C5-C13-C15-C17	-0.03
C15-C17	1.40	C7-C17-H18	125.21	C7-C5-C13-C15	-179.98
C17-C7	1.40	C15-C17-H18	126.25	C5-C7-C17-C15	-179.99
C7-C5	1.49	C15-C17-H16	126.04	C17-C7-C6-C4	-179.98
C7-C6	1.38	C13-C15-H16	125.05	C2-C3-C5-C13	-179.98
C6-C4	1.39	C15-C13-H14	126.25	C13-C5-C7-C6	179.98
C1-H8	1.08	C5-C3-H10	115.28	C3-C5-C7-C17	179.99
C2-H9	1.08	C2-C3-H10	115.69	C15-C17-C7-C6	0.01
C6-H12	1.08	C3-C2-H9	115.69	C15-C13-C5-C3	-179.97
C17-H18	1.08	C1-C2-H9	115.62	C13-C5-C3-C2	-179.98
C15-H16	1.08	C2-C1-H8	115.07	C5-C13-C15-C17	179.9
C13-H14	1.08	C1-C4-H8	115.07	H16-C15-C17-C7	179.98
C3-H10	1.08	C4-C1-C2	129.89	H16-C15-C13-C5	179.98
		C2-C3-C5	129.01	H16-C15-C17-C7	179.98
		C3-C5-C13	129.10	H14-C13-C15-C17	-179.97
		C3-C5-C7	108.52	H18-C17-C7-C6	0.00
		C13-C15-C17	109.90	H14-C13-C5-C7	-179.98
		C15-C17-C7	108.52	H18-C17-C7-C5	-179.98
		C17-C7-C6	126.11	H12-C6-C7-C17	0.00
		C7-C6-C4	129.01	H10-C3-C5-C7	179.99
		C1-C2-C3	128.68	H10-C3-C5-C13	0.01
				H12-C6-C4-C1	-179.99
				H11-C4-C1-C2	-179.99
				H9-C2-C1-C4	-179.99
				H8-C1-C4-C6	179.99
				H11-C4-C6-C7	-179.99

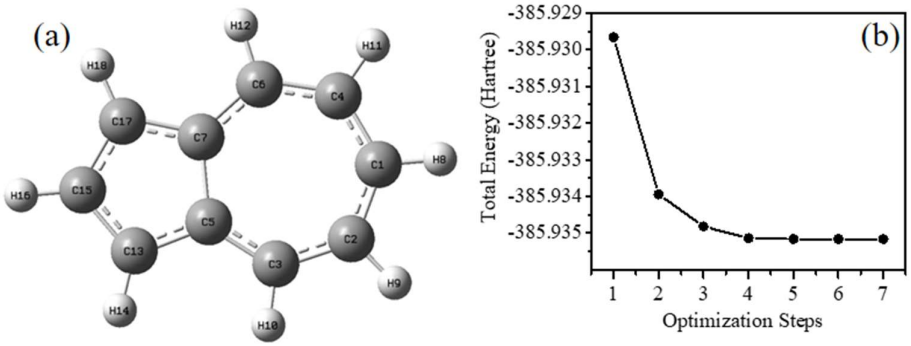

Figure 2: (a) Optimized structure of Azulene molecule having symbol as well as numbering of atoms (b) plot of optimization steps vs total energy.

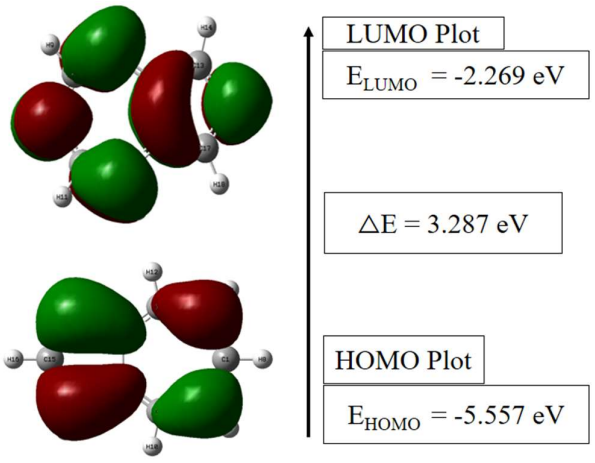

Figure 3: HOMO-LUMO plot and its energy gap of Azulene molecule.

smaller HOMO-LUMO energy gap compared to naphthalene. This reduced gap allows electronic transitions in the visible region, accounting for the characteristic blue color of azulene, whereas naphthalene, with its larger gap, absorbs only in the ultraviolet region and thus appears colorless. This difference arises from the non-uniform charge distribution and intrinsic dipole character of azulene, in contrast to the more symmetric electronic structure of naphthalene [24] .

Density of state (DOS) spectrum

A molecule's electronic structure and general electrical characteristics can be inferred from its density of states (DOS). It describes electronic transitions from the ground state to the lowest unoccupied energy level and shows how electrons are distributed in the valence and conduction bands. [25-27]. Figure 4 represents the DOS spectrum and it provides a clear explanation about the availability of multiple states at various energy levels. The occupied (filled) donor orbitals are represented by the green energy region, whereas the virtual (unfilled) acceptor orbitals are represented by the red energy region. In this DOS spectrum analysis, bonding interactions are represented by positive values, while anti-bonding interactions are represented by negative values. It indicates a non-bonding interaction when the value is zero. [28]. In this Figure 4, the azulene molecule observed energy gap in the DOS spectrum is 3.257 eV, which is nearly equal to the HOMO-LUMO energy gap, i.e. 3.287 eV, and demonstrates good agreement in between them.

Mulliken charge distribution

Mulliken atomic charges, which were determined using techniques from the realm of quantum science, provide an explanation for the distribution of electrons across different atomic orbitals [29]. Mulliken atomic charge values influence the electronic structure, dipole moment molecular polarizability and many other characteristics of the molecular system. The electrical charge of the atom affects the molecular shape and bonding arrangement [28]. Figure 5 shows a histogram of the Mulliken charge distribution for each atom of the title molecule. It is observed that every hydrogen atom together with C5 and C7 in this title molecule have positive charges indicating that they are susceptible to a nucleophilic attack. Because of their ability to accept charge, the hydrogen atom exhibits a net positive charge associated with the carbon as seen in the charge distribution [17]. Besides this, every carbon atom has negative charge except C5 and C7.

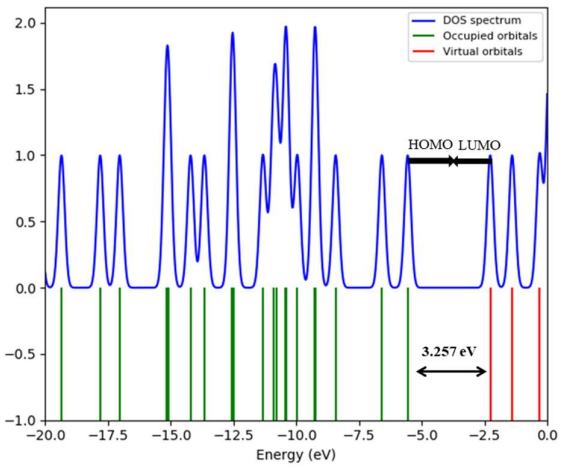

Figure 4: Density of states (DOS) spectrum of title molecule.

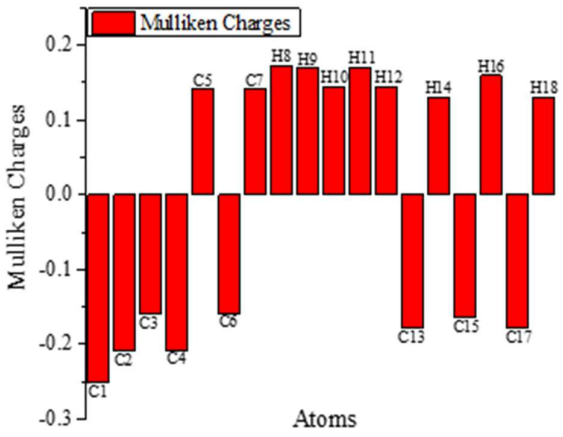

Figure 5: Mulliken charge distribution chart for Azulene molecule.

They have positive charge indicating that they are susceptible to an electrophilic attack on the negative side. It is found that the negative charges on the Carbon atoms are due to their electron withdrawing and donating nature. In the Figure 5, H8 and H11 exhibit the highest positive charge, while the C1 and C2 exhibit the highest negative charge.

The higher positive Mulliken charges on H8 and H11 indicate significant electron deficiency at these sites. This suggests enhanced bond polarization, making these hydrogens more acidic and susceptible to intermolecular interactions such as hydrogen bonding. Furthermore, the associated atoms bonded to these hydrogens may act as reactive centers for nucleophilic attack, highlighting their potential role in chemical reactivity [30].

Global reactivity descriptors

In order to further our comprehension of the characteris tics of azulene, this study offers range of chemical reactivity measurements as well as details on the stability of the molecular structure [31]. We include the global parameters such as electron nization potential (I), electron affinity (A), chemical potential (μ), electronegativity (χ), hardness (η), softness (S), and global electrophilicity (ω) using the values of ionization potential (I) and electron affinity (A) obtained from the B3LYP/ 6-311G++(d,p) basis set. The values for Ionization Potential ($I = -E_{HOMO}$) and Electron Affinity ($A = -E_{LUMO}$) are found to be 5.557 eV and 2.269 eV, respectively, for azulene. A molecule's potential energy is measured by its chemical potential (μ). The value for the chemical potential (μ) is found to be -3.913 eV and this negative value of chemical potential for the title molecule indicates that the molecule is more prone to react or release energy [17]. The molecule's electronegativity (χ), calculated to be 3.931 eV, indicates its ability to attract electrons. The greater and positive value obtained informs strong tendency to attract electrons in a chemical bond [28]. The azulene molecule's computed global hardness (η) of 1.644 eV shows how stable and resistant the molecule is to change or deforming its lowest or occupied orbital state, also known as its electronic configuration as a result of chemical reactions [13]. Softness (S) is the inverse of hardness and has a value of 0.608 eV^{-1}. It refers to a molecule's polarizability and ease of electron transfer, or its capacity to donate or accept electrons [12]. The global electrophilicity index (ω) has a value of 4.656 eV and it helps predicting how reactive a material will be toward nucleophiles in chemical processes. It defines an atom's or molecule's propensity to take an electron in a chemical reaction. Azulene's electrophilic index (ω) value i.e. 4.656 eV is higher than 1.5 eV and it informs hat it is a strong electrophile [28,32].

Molecular electrostatic potential (MEP), electrostatic surface potential (ESP) and electron density (ED) analysis

The molecular electrostatic potential (MEP) represents the

electrostatic field produced by the combined distribution of electrons and nuclei at any point in the space surrounding a molecule. It serves as a useful indicator of chemical reactivity, as regions of positive potential are susceptible to nucleophilic attack, whereas regions of negative potential favor electrophilic interactions [33,34]. The MEP surface also illustrates the molecule's size, shape, and variation in electrostatic potential across its surface. Moreover, it is closely related to important molecular properties such as dipole moment, electronegativity, partial atomic charges, and overall polarity, thereby providing comprehensive insight into charge distribution and reactive behavior [21].

Fig. 6(a) represents the MEP map with potential value ranging from -2.603 e-3 a.u. (red) to 2.603 e-3 a.u. (blue) following the areas with a negative electrostatic potential represented by red and yellow together with the areas of a positive electrostatic potential shown in blue color. This Figure 6(a) shows that the region around the carbon ring with the red surface (nucleophilic region) suggests the negative potential whereas the positive potential lies on the remaining surface indicating the blue surface (electrophilic region). The energy of a positive charge interacting with the electrons and nuclei of a molecule is termed the electrostatic surface potential [19,21]. Fig. 6(b) shows the ESP surface (mapped on an iso-density surface) with values ranging from 2.897e-3 (red) to 2.897e-3 (blue). The red color suggests a higher negative charge, while the blue color indicates a higher positive charge. As illustrated in Fig. 6(b), the ESP map shows that the negative potential is predominantly distributed around the carbon atoms, appearing as red-yellowish regions and indicating susceptibility to electrophilic attack. The remaining surface exhibits positive potential, suggesting a tendency toward nucleophilic interactions. Figure 6(c) corresponds to electron density plot of azulene and it shows the uniform charge distribution.

Spectroscopic analysis

Vibrational analysis of Azulene molecule in FT-IR spectrum

The different vibrational modes originate from the interaction between the material and infrared radiation, which is governed by the relationship between the wavelength and frequency of the incident infrared light. [35]. For a molecule containing *N* atoms, the maximum number of normal vibrational modes is given by (3N-6) [12,28]. Since the Azulene ($C_{10}H_8$) molecule consists of 18 atoms, it exhibits a total of 48 vibrational modes. The azulene molecule exhibits major vibrational modes such as stretching, rocking, and scissoring, as well as symmetric and asymmetric modes. Figure 7 shows the FT-IR spectrum for Azulene molecule. All the theoretical vibrational frequencies for B3LYP/6-311++G (d, p) have been scaled down by 0.967.

C-H Vibration

The nature of carbon-hydrogen stretching vibrational mode is identified by observing in the region between 2800-3300 cm^{-1} [36,37]. In our titled molecule, the C-H stretching vibrations are observed at 3116.35, 3107.61, 3090.93, 3062.29, 3080.56, 3036.24, 3028.13 and 3026.63 cm^{-1} in the FT-IR spectrum using the B3LYP/6-311G++(d, p) method.

C=C Vibration

The C=C stretching is observed in the range of 1400-1650 cm^{-1} [28,38]. In this case, the C=C vibration are observed at 1585.88, 1575.98, 1525.10, 1477.93, 1437.18, 1434.45, 1378.65, 1372.08 and 1291.69 cm^{-1} in the FT-IR spectrum.

Thermodynamic parameters analysis

The thermodynamic parameters are used to study the thermodynamic properties [39], and this thermodynamic changes are observed with respect to the temperature variations using the software called Moltran program. Various thermodynamic parameters, including the state and direction of a chemical reaction are assessed using enthalpy, Gibbs free energy, and entropy. Figure 8(a indicate the correlation graphs between specific heat capacity at constant volume (C_V) and heat capacity at constant pressure (C_p) with respect to temperature range of 0 K to 500 K. It shows that the C_V and C_p increase along

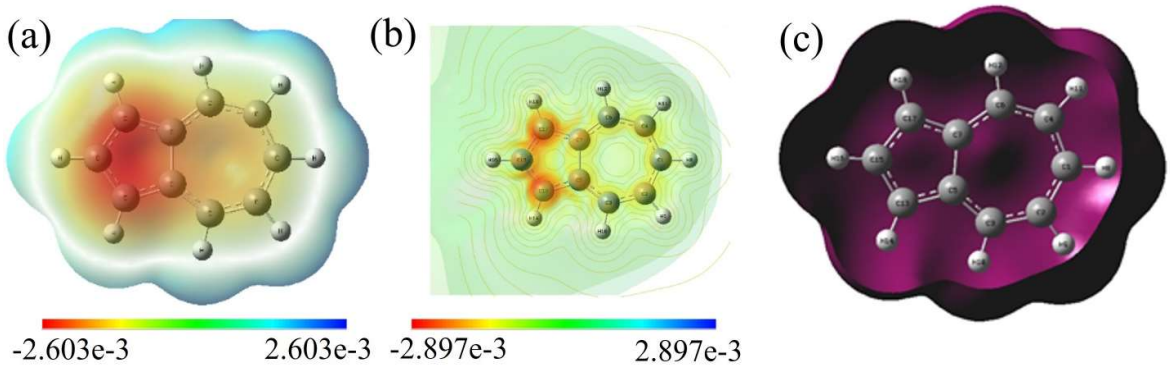

Figure 6: (a) Molecular electrostatic potential (MEP), (b) Electrostatic surface potential (ESP) and (c) Electron density (ED).

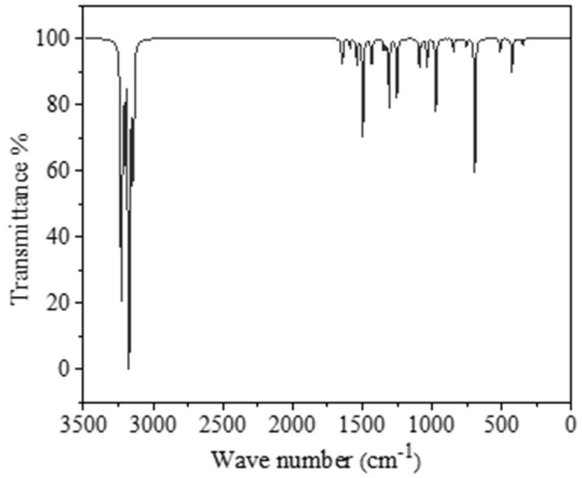

Figure 7: IR spectroscopy for Azulene molecule.

with increase in temperature. Figure 8(b) represents the graph of internal energy (U) and enthalpy (H) with respect to temperature in the range of same temperature. It shows that the U and H also increase with increase in temperature. Figure 8(c) shows the Entropy (S) and Gibbs free energy (G) graph against temperature in the range of 0 K to 500 K where Entropy (S) increases with increase in temperature. However, depending on the enthalpy (H) and entropy (S) of the system, the Gibbs free energy (G) gradually decreases as the temperature increases. The correlation plot between G and S shows that the two curves intersect at a particular point illustrating the relationship between the entropy and Gibbs free energy. The intersection point in figure 8(c) shows the exact temperature at which a system's thermodynamic driving forces change. Specifically, it indicates the point of phase change or chemical equilibrium [40,41].

Conclusion

Density functional theory with the B3LYP method and a 6-311G++(d,p) basis set was used to explore the molecular structure, electronic properties, spectroscopic characteristics, and thermodynamic properties of azulene. Optimization of the molecular geometry produced a set of optimized structures with bond lengths between 1.08 Å and 1.49 Å, providing excellent support for the stability of the ground state configuration, with an optimized energy value of -385.935 Hartree (-10501.291 eV). Azulene was determined to have a HOMO-LUMO energy gap of 3.287 eV hence low chemical reactivity under normal conditions. This result is supported by the density of states spectral data which shows an energy gap of 3.257 eV, providing further correspondence with the frontier molecular orbital investigation. Mulliken charge distributions showed that every hydrogen atom has positive charge indicating susceptibility for nucleophilic attack as well as C5 and C7 and each of the remaining carbon atoms exhibited negative charge which indicated propensity for electrophilic interaction. The global reactivity indices of azulene with its ionization potential 5.557 eV, electron affinity 2.269 eV, and chemical potential -3.931 eV indicate its strong tendency to participate in reactions, with an electrophilicity index of 4.656 eV classifying it as a strong electrophile. Molecular electrostatic potential mapping identified nucleophilic attack as well as C5 and C7 and each of the remaining carbon atoms exhibited negative charge which indicated propensity for electrophilic interaction. The global

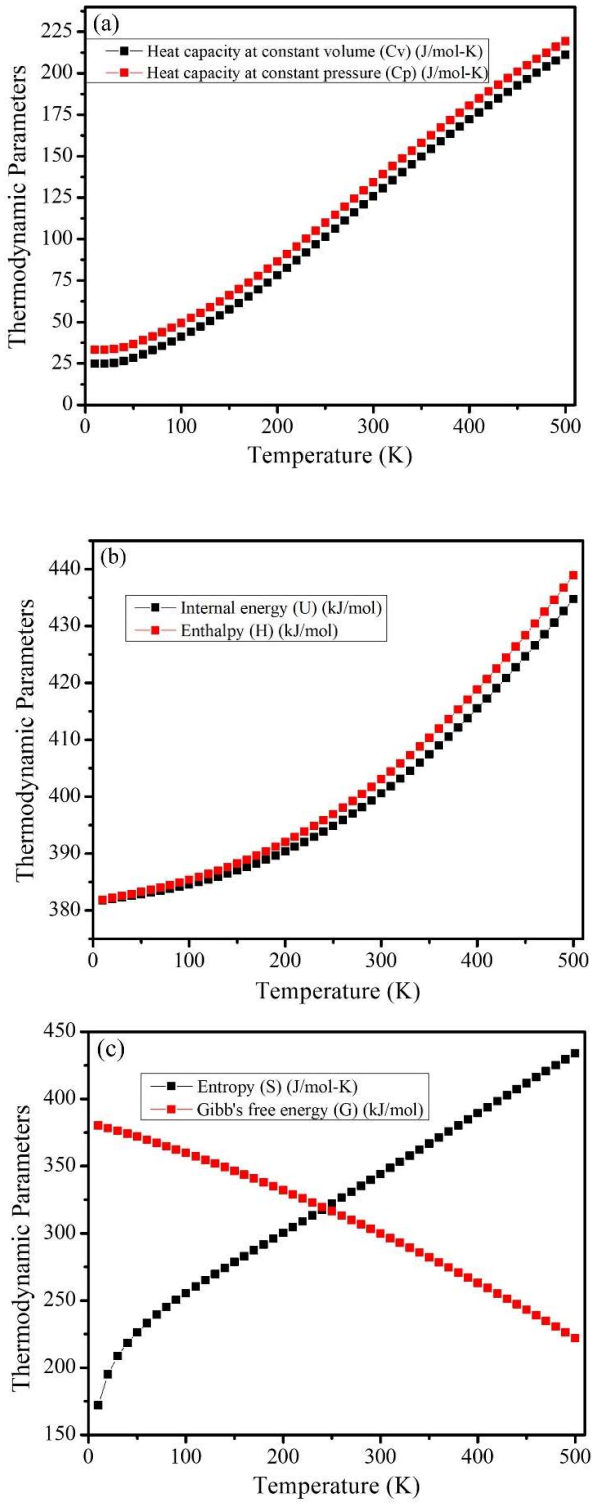

Figure 8: (a) plot of thermodynamic parameters, specific heat capacity at constant volume (C_v) and specific heat capacity at constant pressure (C_p) with respect to temperature, (b) correlation plot of thermodynamic parameters, internal energy (U) and enthalpy (H) with respect to temperature and (c) plot of thermodynamic parameters, Entropy (S) and Gibbs free energy (G) with respect to temperature.

reactivity indices of azulene with its ionization potential 5.557 eV, electron affinity 2.269 eV, and chemical potential -3.931 eV indicate its strong tendency to participate in reactions, with an electrophilicity index of 4.656 eV classifying it as a strong electrophile. Molecular electrostatic potential mapping identified nucleophilic regions (red) around the carbon rings and electrophilic regions (blue) on the remaining molecular surface, further elucidating the charge distribution patterns that govern reactive behavior. Vibrational spectroscopic analysis characterized the major vibrational modes, with C-H stretching observed in the 3129-3222 cm^{-1} region and C=C stretching vibrations identified between 1335-1640 cm^{-1}. Thermodynamic parameter analysis across the temperature range of 0-500 K revealed that heat capacity (both C_V and C_P), internal energy, enthalpy, and entropy increase monotonically with temperature, while Gibbs free energy progressively decreases providing azulene's behavior under varying thermal conditions. This study addresses the existing research gap by delivering a comprehensive theoretical characterization of azulene, establishing a foundation for future experimental studies and its potential applications in pharmaceutical development, molecular electronics, and materials science.

Data Availability Statement

The data supporting the findings of this study can be obtained from the corresponding author with a reasonable request.

Acknowledgements

We would like to express our special thank to Department of Physics, Patan Multiple Campus, Tribhuvan University, Kathmandu for providing necessary help for conducting this research.

References

[1] Szalewicz, K. 2014. Determination of structure and properties of molecular crystals from first principles. *Accounts of Chemical Research*. **47**(11): 3266-3274.
Doi: https://doi.org/10.1021/ar500275m

[2] Hashimoto, S. and Tahara, K. 2022. Theoretical study on the structures, electronic properties, and aromaticity of thiophene analogues of Anti-Kekulene. *Chemistry*. **4**(4): 1546-1560.

Doi: https://doi.org/10.3390/chemistry4040102

[3] Slon, E., Slon, B. and Kowalczuk, D. 2024. Azulene and its derivatives as potential compounds in the therapy of dermatological and anticancer diseases: new perspectives against the backdrop of current research. *Molecules*. **29**(9): 2020.
Doi: https://doi.org/10.3390/molecules29092020

[4] Xin, H., Hou, B. and Gao, X. 2021. Azulene-based π-functional materials: design, synthesis, and applications. *Accounts of Chemical Research*. **54**(7)**:** 1737-1753.
Doi: https://doi.org/10.1021/acs.accounts.0c00893

[5] Klan, P. and Wirz, J. 2009. *Photochemistry of organic compounds: from concepts to practice*. First edition, John Wiley & Sons, Chichester.

[6] Shoji, T. and Ito, S. 2025. Recent progress in the chemistry of ring-fused azulenes: synthesis, reactivity and properties. *Chemistry–An Asian Journal*. **20**(9): e202500166.
Doi: https://doi.org/10.1002/asia.202500166

[7] Zeng, H. N., Png, Z. M. and Xu, J. 2020. Azulene in polymers and their properties. *Chemistry–An Asian Journal*. **15**(13): 1904-1915.
Doi: https://doi.org/10.1002/asia.202000444

[8] Hajialiakbari, N., Seaidian, H., Mirjafary, Z. and Mokhtari, J. 2024. Valuable insights into the structural, electronic, and aromaticity aspects of azulene and its monophospha-derivatives. *Computational and Theoretical Chemistry*. **1235**: 114571.
Doi: https://doi.org/10.1016/j.comptc.2024.114571

[9] El-Demerdash, S. H. and Gad, S. F. 2020. A computational study of gas-phase acidity and basicity of azulene-based uracil analogue. *Structural Chemistry*. **31**(1): 319-328.
Doi: http://doi.org/10.1007/s11224-019-01408-8

[10] El-Nahas, A. M., Staykov, A. and Yoshizawa, K. 2016. First principles calculations of electron transport through azulene. *The Journal of Physical Chemistry C*. **120**(17): 9043-9052.
Doi: https://doi.org/10.1021/acs.jpcc.6b00767

[11] Xin, H. and Gao, X. 2017. Application of azulene in constructing organic optoelectronic materials: New tricks for an old dog. *ChemPlusChem*. **82**(7): 945-956.
Doi: https://doi.org/10.1002/cplu.201700039

[12] Uprety, R., Ghimire, R., Gharti Magar, P., Rokka, D., Khadka, I. B., Neupane, R. and Rai, K. B. 2024. Study of the molecular structure, electronic structure, spectroscopic analysis and thermodynamic properties of dibenzofuran using first principles. *Journal of Nepal Physical Society*. **10**(2): 8-18.
Doi: https://doi.org/10.3126/jnphyssoc.v10i2.79470

[13] Kaya, S. & Kaya, C. 2015. A new method for calculation of molecular hardness: a theoretical study. *Computational and theoretical chemistry*. **1060**: 66-70.
Doi: https://doi.org/10.1016/j.comptc.2015.03.004

[14] Matamala, A. R. and Alarcón, A. A. 2012. A simple model for the calculation of HOMO and LUMO energy levels of benzocatafusenes. *International Journal of Quantum Chemistry*. **112**(5): 1316-1322.
Doi: https://doi.org/10.1002/qua.23135

[15] Cairo, R. R., Stevens, A. M. P., de Oliveira, T. D., Batista, A. A., Castellano, E. E., Duque, J. and Erben, M. F. 2017. Understanding the conformational changes and molecular structure of furoyl thioureas upon substitution. *Spectrochimica Acta Part A: Molecular and Biomolecular Spectroscopy*. **176:** 8-17.
Doi: https://doi.org/10.1016/j.saa.2016.12.038

[16] Bishwokarma, N., Budha, C., Teemilsina, N. K. and Rai, K. B. 2025. Exploring vibrational spectra, electronic properties and thermal analysis of Isoguanine molecule using DFT. *Scientific World*. **18**(18): 5-14.
Doi: http://doi.org/10.3126/sw.v18i18.78512

[17] Magar, A. R., Ghimire, R., Basnet, B., Shrestha, P. M., Gupta, S. P. and Rai, K. B. 2024. First-principles calculation of cumene: molecular structure, electronic structures, spectroscopic analysis, and thermodynamic properties. *Molung Educational Frontier*. **14**: 1-26.
Doi**:** https://doi.org/10.3126/mef.v14i01.67890

[18] Tsuchiya, T., Higashibeppu, M. and Mazaki, Y. 2023. Synthesis and properties of twisted and helical azulene oligomers and azulene-based polycyclic hydrocarbons. *Chemistry Ope*n. **12**(11): e202100298.
Doi: https://doi.org/10.1002/open.202100298

[19] Akman, F. 2019. A density functional theory study based on monolignols: molecular structure, HOMO-LUMO analysis, molecular electrostatic potential. *Transport.* **1**: 2.
Doi: https://doi.org/10.35812/cellulosechemtechnol.2019.53.-24

[20] Khadka, I. B., Rai, K. B. and Rokka, D. 2025. Low-power light irradiation based plasmonic photoresponse on quasi-freestanding monolayer/AuNPs hybrid system. *Indian J Phys*. **99**(1): 95-103.
Doi: https://doi.org/10.1007/s12648-024-03254-9

[21] Mohamed, A., Visco Jr, D. P., Breimaier, K. and Bastidas, D. M. 2025. Effect of molecular structure on the B3LYP-computed HOMO–LUMO gap: a structure− property relationship using atomic signatures. *ACS omega*. **10**(3): 2799-2808.
Doi: https://doi.org/10.1021/acsomega.4c08626

[22] Rai, K. B. and Yadav, R. P. 2022. Raman spectroscopy investigation on semi-curve woven fabric-graphene synthesized by the chemical vapor deposition process. *Jordan Journal of Phys.* **15**(2): 169-77.
Doi: https://doi.org/10.47011/15.2.7

[23] Abraham, C. S., Prasana, J. C., Muthu, S. and Raja, M. 2018. Quantum computational studies, spectroscopic (FT-IR, FT-Raman and UV–Vis) profiling, natural hybrid orbital and molecular docking analysis on 2, 4 Dibromoaniline. *Journal of Molecular Structure*. **1160:** 393-405.
Doi: https://doi.org/10.1016/j.molstruc.2018.02.022

[24] Novak, I. 2017. Distorted naphthalenes and azulene. *Computational & Theoretical Chemistry*. **1117**: 251-257.
Doi: http://dx.doi.org/10.1016/j.comptc.2017.08.007

[25] Shin, H. C., Ahn, S. J., Kim, H. W., Moon, Y., Rai, K. B., Woo, S. H. and Ahn, J. R. 2016. Room temperature deintercalation of alkali metal atoms from epitaxial graphene by formation of charge-

transfer complexes. *Applied Physics Letters.* **109**(8): 0816. Doi:10.1063/1.4961633

[26] Yadav, R. P. and Rai, K. B. 2024. Tailoring of ZnO thin films: effect of number of coating and sample ageing. *International Journal of Mathematics and Physics*. **14**(2): 95–102. Doi: https://doi.org/10.26577/ijmph.2023.v14.i2.011

[27] Yadav, R. P., Rai, K. B. and Shrestha, S. P. 2021. Electrical and optical properties of dip coated Al-doped ZnO thin films: effect of Al-concentration, starting solution and sample ageing. *Mongolian Journal of Chemistry.* **22**(48): 38-44. Doi: https://doi.org/10.5564/mjc.v22i48.1743

[28] Thapa, D., Rai, K. B., Pandey, B. and Ghimire, M. P. 2025. Molecular insights into Herniarin: Structural, spectroscopic, electronic and thermodynamic characterization via density functional theory. *Himalayan Physics*. **12**(1): 64-83. Doi: https://doi.org/10.3126/hp.v12i1.86388

[29] Govindasamy, P., Gunasekaran, S. and Srinivasan, S. 2014. Molecular geometry, conformational, vibrational spectroscopic, molecular orbital and Mulliken charge analysis of 2-acetoxybenzoic acid. *Spectrochimica Acta Part A: Molecular and Biomolecular Spectroscopy*. **130**: 329-336. Doi: https://doi.org/10.1016/j.saa.2014.03.056

[30] Chimarro-Contreras A, Lopez-Revelo Y, Cardenas-Gamboa J. and Terencio T. 2024. Insights into the effect of charges on hydrogen bonds. *Int J Mol Sci*. **25**(3): 1613. Doi**:** https://doi.org/10.3390/ijms25031613.

[31] Vijayaraj, R., Subramanian, V. and Chattaraj, P. K. 2009. Comparison of global reactivity descriptors calculated using various density functionals: a QSAR perspective. *Journal of chemical theory and computation*. **5**(10): 2744-2753. Doi: https://doi.org/10.1021/ct900347f

[32] Jerbi, J. and Springborg, M. 2017. Computational study of the reactivity of cytosine derivatives. *Journal of Computational Chemistry*. **38**(14): 1049-1056. Doi: https://doi.org/10.1002/jcc.24781

[33] Murray, J. S. and Politzer, P. 2017. Molecular electrostatic potentials and noncovalent interactions. *Wiley Interdisciplinary Reviews: Computational Molecular Science*. **7**(6): e1326. Doi: https://doi.org/10.1002/wcms.1326

[34] Basnet, B., Rana Magar, A., Ghimire, R., Joshi, U. and Rai, K. B. 2024. First-principles calculations to investigate structural, spectroscopic features, electronic and thermodynamic properties of trichloroacetal-dehyde. *Himalayan Journal of Science and Technology*. **8**(1): 1-9. Doi: https://doi.org/10.3126/hijost.v8i1.83091

[35] Rai, K. B., Khadka, I. B., Koirala, A. R. and Ray, S. K. 2021. Insight of cleaning, doping and defective effects on the graphene surface by using methanol. *Advances in Materials Research*. **10**(4): 283-92. Doi: https://doi.org/10.1016/j.optmat.2023.113836

[36] Sebek, J., Knaanie, R., Albee, B., Potma, E. O. and Gerber, R. B. 2013. Spectroscopy of the C–H stretching vibrational band in selected organic molecules. *The Journal of Physical Chemistry A*. **117(**32): 7442-7452. Doi: https://doi.org/10.1021/jp4014674

[37] Budha, C. and Rai, K. B. 2024. Study of the molecular structure, spectroscopic analysis, electronic structures and thermodynamic properties of niacin molecule using first-principles. *Journal of Nepal Chemical Society*. **44**(2): 1–12. Doi: https://doi.org/10.3126/jncs.v44i2.68263

[38] Abkari, A., Chaabane, I. and Guidara, K. 2016. DFT (B3LYP/LanL2DZ and B3LYP/6311G+(d, p)) comparative vibrational spectroscopic analysis of organic–inorganic compound bis (4-acetylanilinium) tetrachlorocuprate (II). *Physica E: Low-dimensional Systems and Nanostructures*. **81**: 136-144. Doi: https://doi.org/10.1016/j.physe.2016.03.010

[39] Benamrani, A., Daoud, S., Salam, M. M. A. and Rekab-Djabri, H. 2021. Structural, elastic and thermodynamic properties of YRh: DFT study. *Materials Today Communications*. **28:** 102529. Doi: https://doi.org/10.1016/j.mtcomm.2021.102529

[40] Ojha, T., Shrestha, P. M., Gupta, S. P. and Rai, K. B. 2025. Quantum chemical insights into the electronic, vibrational and thermodynamic properties of chloro-substituted anisole. *Al-Nahrain Journal of Science*. **28**(4): 146-164. Doi: https://doi.org/10.3126/hijost.v7i1.61128

[41] Gharti Magar, P., Uprety, R. and Rai, K. B. 2024. First-Principles DFT study of the molecular structure, spectroscopic analysis, electronic structures and thermodynamic properties of ascorbic acid. *Himalayan Physics*. **11**(1): 28-40. Doi: https://doi.org/10.3126/hp.v11i1.65329